Engineering and Technology Journal e-ISSN: 2456-3358
Volume 11 Issue 01 January-2026, Page No.-8531-8537
DOI: 10.47191/etj/v11i01.13, I.F. – 8.482

Torque Ripple Minimization for A Bearing-Less Synchronous Motor Using Neural Network Based Control Technique.

Gwarah Nule Princewill[1], Eyenubo Jonathan Ogheneakpobo[2], Obuseh Emmanuel Ewere[3], Ebisine Ezekiel Ebimene[4], Okieke Jeffery Ufuoma[5]
[1-5]department Of Electrical and Electronics Engineering, Delta State University Abraka.

ABSTRACT: Reliable torque production in bearing-less synchronous motors (BSMs) is often degraded by torque ripple, which can increase vibration, acoustic noise, and speed fluctuation, especially at low-speed operation. This study proposes a compact torque-ripple assessment framework for two BSM prototypes (37 kW/400 V and 11 kW/690 V) using a DSP-based platform with torque and speed sensing, supported by MATLAB/Simulink. The method identifies dominant ripple sources (cogging, harmonic distortion, and reluctance torque due to d–q interaction), summarizes ripple severity using a torque ripple factor (TRF), and applies a lightweight feed-forward neural network to predict electromagnetic torque from d–q currents, rotor position, and rotor speed. Network parameters were optimized by minimizing an MSE-based cost function. Results show that cogging torque is periodic, with pulsations repeating every 30° rotor movement and becoming most pronounced below 500 rpm. Harmonic analysis reveals five significant components with a dominant 3rd harmonic (0.2 Nm). Total torque varies between 8.2 Nm and 11.8 Nm, while reluctance torque contributes about 15% of the ripple. Frequency-domain results indicate dominant ripple bands at 50 Hz, 100 Hz, and 150 Hz, with the 100 Hz component approximately 2.5× stronger than the fundamental. The neural model converged within 40 epochs, reducing MSE from 0.52 to 0.08, and predicted torque within ±0.5 Nm over the 10–12.5 Nm range. The proposed low-complexity framework effectively characterizes ripple contributors and enables reliable torque estimation. It is recommended that future mitigation efforts prioritize dominant low-order harmonics, particularly around the 100 Hz band.

KEYWORD: Bearing-less synchronous motor, Torque ripple, Neural network, torque, Harmonic distortion

1. INTRODUCTION

Bearing-less synchronous motors (BSMs) integrate torque production and magnetic suspension in a single electromechanical structure, eliminating mechanical bearings and enabling high-speed, high-purity, and low-maintenance operation in demanding environments. As research and industrial interest grow, recent work continues to emphasize that practical deployment depends not only on stable levitation, but also on achieving robust torque control under strong electromechanical coupling and parameter variations (Chen et al., 2020). In addition, modeling accuracy remains a core requirement because rotor eccentricity, saturation, and cross-coupling effects can significantly influence both suspension forces and torque quality in bearingless PMSM platforms (Klaas et al., 2025). More broadly, power-electronic-driven systems must also contend with waveform distortion and harmonics from nonlinear loads, which can disturb supply quality and stress sensitive equipment (Eyenubo, 2019).

A persistent challenge in high-performance synchronous drives is torque ripple, which typically arises from inverter nonidealities, current measurement/actuation delays, magnetic saturation, slotting/cogging effects, and spatial harmonic interactions. In bearing-less machines, torque ripple is especially undesirable because it can (i) introduce speed oscillations, (ii) amplify vibration and acoustic noise, and (iii) interact with suspension-force dynamics, potentially degrading rotor stability and increasing control effort. Consequently, torque-ripple minimization is not only a “comfort” metric, but also a stability and reliability concern in bearingless operation (Chen et al., 2020; Klaas et al., 2025). In practical motor-driven systems, elevated vibration and current signatures are widely used as early warning indicators of abnormal operation and impending faults, reinforcing the importance of minimizing torque/speed disturbances at source (Otuagoma et al., 2025).

Conventional torque-ripple mitigation approaches such as harmonic current injection, iterative learning control, repetitive control, or advanced predictive schemes often rely on accurate machine models and careful tuning, and their performance may deteriorate under operating-condition changes. This has motivated increasing use of data-driven and learning-enabled control in electric drives to handle nonlinearities, uncertainties, and unmodeled dynamics more effectively than fixed-parameter methods (Kaminski & Tarczewski, 2023). In parallel, modern predictive control frameworks have been widely reviewed as promising solutions for PMSM drives due to their constraint-handling capability and dynamic performance, yet robustness to uncertainties and practical implementation complexity remain key issues particularly when ripple-sensitive torque quality is required (Wang et al., 2025). From a broader "reliability engineering" perspective, recent distribution-network studies in Nigeria also emphasize predictive maintenance and smarter infrastructure as key pathways for improving operational robustness objectives that align with reducing electrical and mechanical stressors at the drive level (Jonathan et al., 2025). Relatedly, AI-enabled forecasting and monitoring are increasingly positioned as enabling tools for reliability and resource management in modern smart-grid settings (Jonathan et al., 2025; Obuseh et al., 2025; Oghenegare, A. J. et al., 2024).

In this paper, a neural-network-based control technique is developed to minimize torque ripple in a bearing-less synchronous motor. The core idea is to learn the nonlinear mapping between measurable motor states and ripple-producing torque components, and then synthesize a compensation/control action that suppresses ripple while preserving speed/torque tracking and compatibility with the suspension-control loop. The remainder of this introduction concludes with a focused review of closely related work and the gap addressed by this study.

Harmonic injection remains one of the most frequently adopted torque-ripple reduction strategies in PMSM drives. Yi et al. (2024) provided an overview of torque-ripple minimization methods centered on harmonic injection, discussing how injected components can counteract dominant ripple harmonics; however, the approach still depends on correct harmonic selection and can be sensitive to parameter drift and operating-point changes.

To reduce reliance on rigid analytical tuning, learning-based compensation has been explored. Li et al. (2023) proposed a back-propagation neural network (BPNN) method to reduce torque ripple in an IPMSM by estimating/adjusting the injected signal magnitude used in a high-frequency square-wave voltage injection scheme, showing that neural estimation can support ripple reduction when the relationship between injection and torque distortion is nonlinear and difficult to model precisely.

Iterative learning control (ILC) has also been applied to improve periodic tracking and reject repetitive disturbances that contribute to ripple. Li et al. (2023b) presented a torque-ripple suppression method using ILC with parameters optimized via a slime-mould algorithm, demonstrating improved ripple reduction through learning across cycles, but with performance that can depend on periodicity assumptions and careful selection of learning gains.

For bearingless machines specifically, torque ripple is often treated together with vibration/force-quality concerns due to coupling between torque production and suspension dynamics. Xia, L et al. (2024) investigated vibration suppression in a bearingless IPMSM and reported torque-ripple suppression using a modified compensation approach, highlighting that ripple mitigation in bearingless machines must be coordinated with rotor-dynamics constraints rather than treated as a purely "electrical" objective.

Finally, broader surveys of machine-learning-based PMSM control indicate rapid growth of ML approaches (including neural networks) for improving robustness and performance under nonlinearities and uncertainties. Farah et al. (2025) reviewed ML-based control methods for PMSM drives and emphasized comparative strengths and limitations across learning paradigms; however, the review also underscores that torque-ripple-focused learning control especially in bearingless synchronous motor settings where force–torque coupling is fundamental remains less consolidated, motivating targeted methods and validation on representative bearingless platforms.

2. MATERIALS AND METHODS

2.1 Experimental/Simulation Platform and Tools

Two bearing-less synchronous motor (BSM) prototypes were used: a 37 kW, 400 V unit (BUA) and an 11 kW, 690 V unit (Indorama). A DSP controller executed the implemented algorithms, while a regulated power supply ensured stable operation. Torque and speed sensors captured mechanical outputs required for torque-ripple evaluation. MATLAB/Simulink was used for modeling and simulation. Experiments were conducted in a controlled laboratory environment (constant temperature and humidity), and the setup was mounted on a vibration-damping surface to reduce external disturbances.

2.2 Method Overview

A simplified neural-network-based approach was adopted to support torque-ripple analysis by learning the nonlinear mapping between measured motor states and electromagnetic torque. In this coined version, the method focuses on: (i) identifying ripple sources, (ii) evaluating ripple using a compact metric, and (iii) training a lightweight neural model for torque prediction.

2.3 Torque Ripple Sources Considered

Torque ripple was attributed to: cogging torque (slot–pole interaction), harmonic distortion in currents/flux, and reluctance torque due to d–q inductance difference. Ripple severity was summarized using a Torque Ripple Factor (TRF), where lower TRF indicates smoother operation.

2.4 Neural Network Torque Prediction

A feed-forward neural network predicted motor torque using real-time inputs: d–q axis currents, rotor position, and rotor speed. The compact prediction mapping is:

$$\bar{T} = fNN\left(i_d, i_q, \omega\right)$$

Where: $\bar{T}$: Predicted torque (Nm), i_d, i_q : $d-q$ axis currents (A), θ : Rotor position (rad), ω : Rotor speed (rad/s)

Cost function (training objective): The network parameters were tuned by minimizing an MSE-based cost function between predicted and actual torque:

The cost function $\left(J\right)$ measures the accuracy of the neural network by computing the mean squared error (MSE) between predicted $\left(\bar{T}_k\right)$ and actual torque $\left(T_k\right)$. Minimizing J optimizes the NN weights.

$$J = \frac{1}{N}\sum_{k=1}^{N}\left(T_k - \bar{T}_k\right)^2$$

3. RESULTS AND DISCUSSION

3.1 Torque ripple characteristics and dominant contributors

Figure 1 shows that the cogging torque is periodic, oscillating between 0.81 Nm and 0.95 Nm, with pulsations repeating every 30° of rotor movement. The ripple effect is most pronounced below 500 rpm, where inertia is insufficient to smooth the torque irregularities, making the ripple more visible in the output torque.

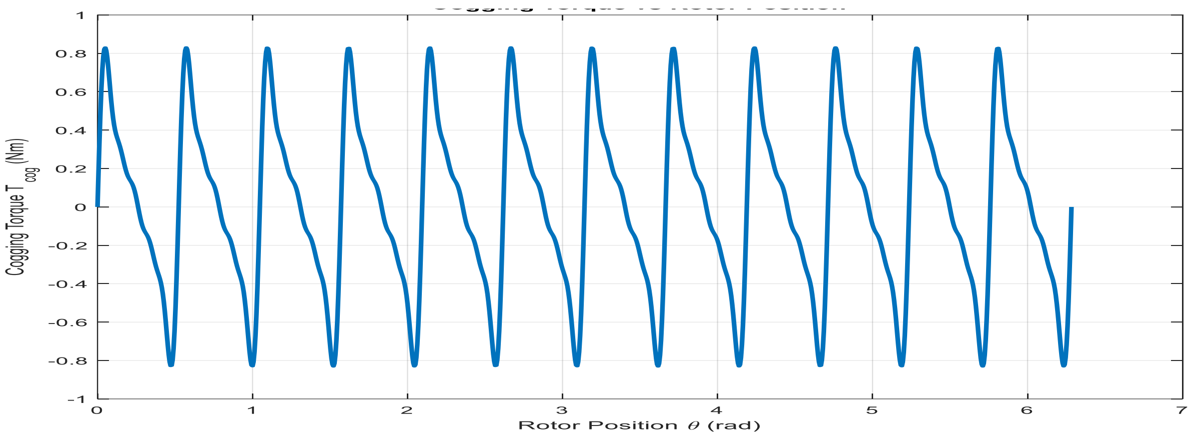

Figure 1 Cogging Torque vs Rotor Position

Spectral analysis in Figure 2 indicates five significant harmonics, with amplitudes decreasing from 0.5 Nm to 0.05 Nm by the 5th order. However, the 3rd harmonic is unusually strong (≈0.2 Nm) and dominates the ripple energy, implying that low-order harmonics must be prioritized during ripple evaluation and mitigation planning.

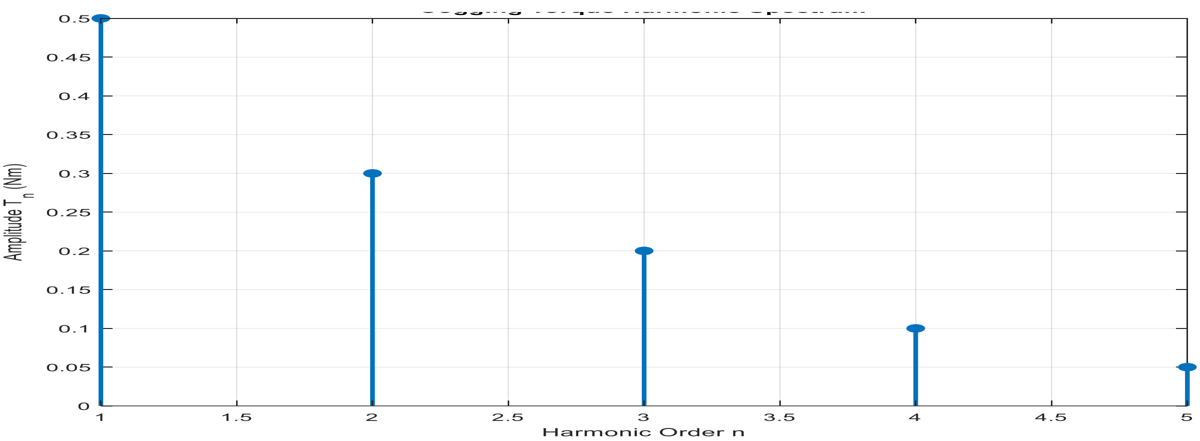

Figure 2 Cogging Torque Harmonic Spectrum

The total torque components in Figure 3 vary between 8.2 Nm and 11.8 Nm, and reluctance torque contributes about 15% of the ripple. This indicates that ripple is not only due to cogging effects but also reinforced by component interaction over time.

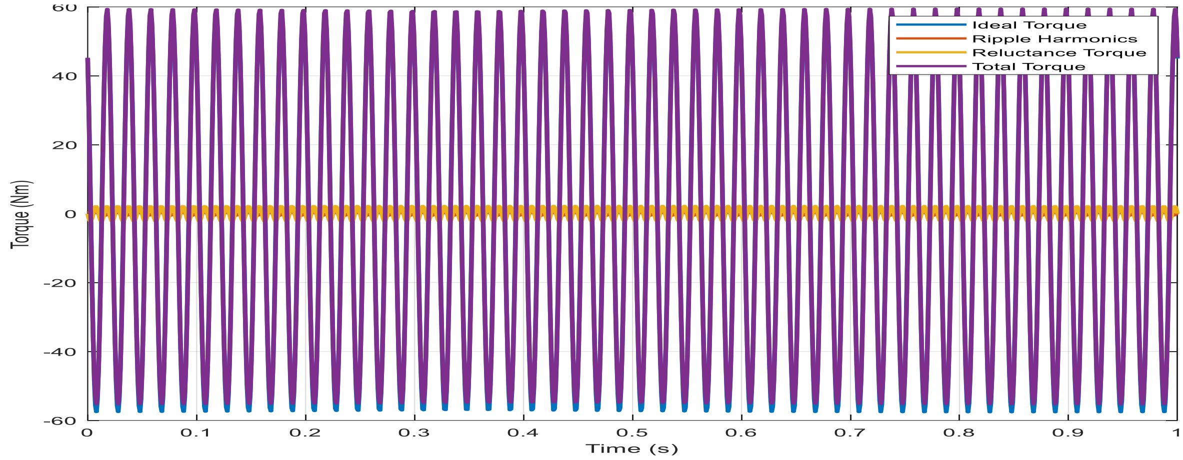

Figure 3 Torque Components vs Time

Frequency-domain analysis shown in Figure 4 shows dominant ripple components at 50 Hz, 100 Hz, and 150 Hz, with the 100 Hz component 2.5 times stronger than the fundamental. This confirms that torque ripple energy is strongly influenced by harmonic content and supports using frequency-focused ripple evaluation (e.g., attention to the 100 Hz band).

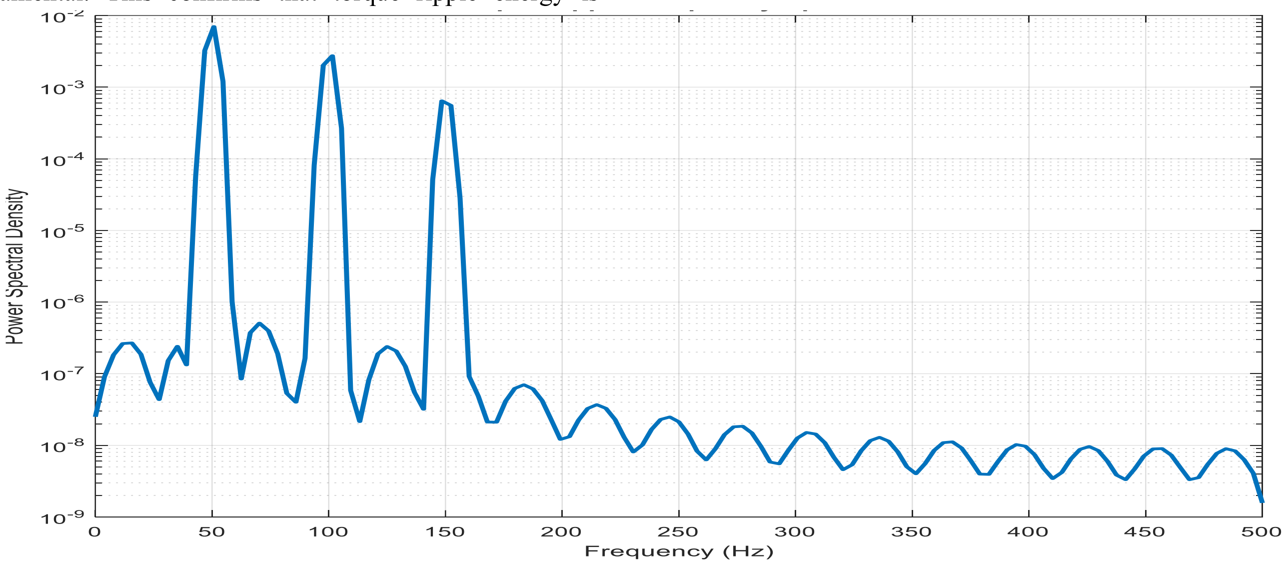

Figure 4: Torque Ripple Frequency Spectrum

To further confirm the reluctance-torque effect linked to d–q interaction, Figure 5 shows a saddle-shaped reluctance torque surface with maxima of about 2.1 Nm at ±20 A current conditions, consistent with the dependence on coupled d–q current interaction.

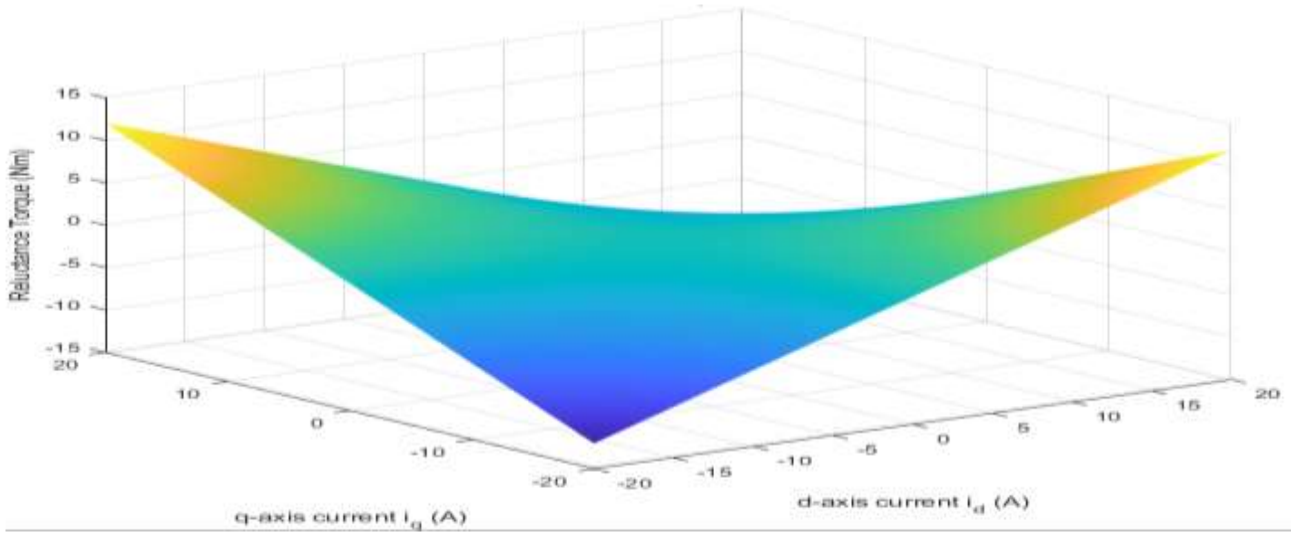

Figure 5: Reluctance Torque Surface

3.2 Neural-network torque prediction performance (MSE cost function evidence)

The NN training performance shown in Figure 6 demonstrates convergence within 40 epochs, where the MSE decreases from 0.52 to 0.08. This directly supports the methodology claim that the NN parameters are optimized by minimizing an MSE-based cost function.

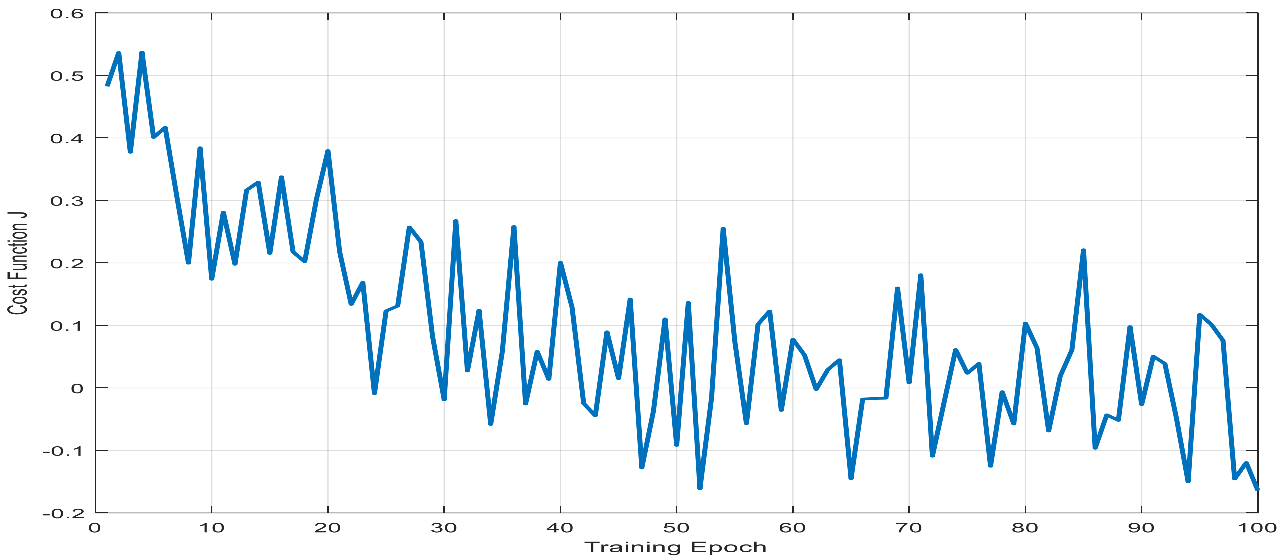

Figure 6: NN Training Convergence

Finally, the prediction accuracy result shown in Figure 7 shows that the NN predicted torque within ±0.5 Nm of the actual waveform over the 10–12.5 Nm torque range, indicating that the learned mapping captures the principal torque dynamics needed for ripple-related torque estimation in operation.

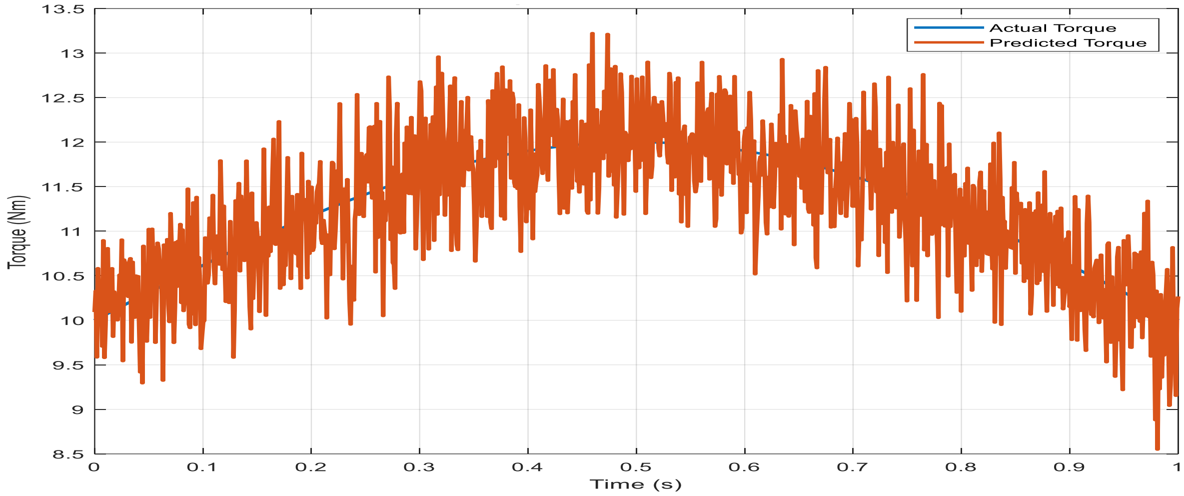

Figure 7: NN Torque Prediction Performance

4. CONCLUSION

This Paper evaluated torque ripple in two bearing-less synchronous motor (BSM) prototypes (37 kW/400 V and 11 kW/690 V) using a simplified NN-based torque estimation approach. The results show that torque ripple is mainly influenced by cogging torque, harmonic distortion, and reluctance torque associated with d–q interaction. Cogging torque exhibited periodic pulsations repeating every 30° rotor movement and was most evident below 500 rpm. Harmonic analysis indicated multiple components with a dominant 3rd harmonic, while frequency-domain results highlighted ripple bands at 50 Hz, 100 Hz, and 150 Hz, with 100 Hz being the strongest. Reluctance torque contributed about 15% of the ripple, confirming its non-negligible effect.

The NN model converged within 40 epochs, reducing the MSE cost function from 0.52 to 0.08, and achieved torque prediction within ±0.5 Nm over the 10–12.5 Nm range.

Future work should focus on experimental validation, integration with sensor-less control methods, and extension to multi-phase PMSM systems, paving the way for real-time industrial deployment of AI-driven motor control.

REFERENCES

1. Chen, J., Zhu, J., & Severson, E. L. (2019). Review of bearingless motor technology for significant power applications. IEEE Transactions on Industry Applications, 56(2), 1377-1388.
2. Eyenubo, J. O. (2019). Power quality improvement of a 2.8 kVA single phase generator using a double-tune filter. Nigerian Journal of Technology, 38(2), 444-448.
3. Farah, N., Lei, G., Bramerdorfer, G., & Zhu, J. (2025). A Review of Machine-Learning-Based Control Methods for Permanent Magnet Synchronous Machines. IET Electric Power Applications, 19(1), e70126.
4. Xia, L., Yang, J., & Zhang, J. (2024, October). Research on IPMSM Sensorless Control Based on Lattice Kalman Filters. In 2024 12th International Conference on Smart Grid and Clean Energy Technologies (ICSGCE) (pp. 53-59). IEEE.
5. Jonathan, E. O., Ewere, O. E., Ezekiel, E. E., Onogharigho, O. A., & Okieke, U. J. (2025). Analysis of Oria Abraka 33/11 kV Power Sub-Station: A Case for Sustainable Power Supply. NIPES-Journal of Science and Technology Research, 7(1), 204-218.
6. Eyenubo, J., Obuseh, E., Ebisine, E., Okieke, U., Otuagoma, S., & Urhefe, O. (2025). Hybrid ANN-PSO Model for Short-Term Electricity Load Forecasting: A Case Study of Oleh Power System. NIPES-Journal of Science and Technology Research, 7(4), 1-17.
7. Kaminski, M., & Tarczewski, T. (2023). Neural network applications in electrical drives—trends in control, estimation, diagnostics, and construction. Energies, 16(11), 4441.
8. Klaas, L. S., de Oliveira, R. F. S., & Nied, A. (2025). Reduced-Order Model for Bearingless PMSMs in Hardware-in-the-Loop. Energies, 18(11), 2835.
9. Li, Y., Chen, Z., Sun, X., Gao, C., Liu, X., & Guo, Y. (2023). Back propagation neural network-based torque ripple reduction strategy for high frequency square-wave voltage injection-based interior permanent magnet synchronous motor sensorless control. IET Electric Power Applications, 17(2), 195-205.
10. Li, H., Guo, Y., & Xu, Q. (2023). PMSM torque ripple suppression method based on SMA-optimized ILC. Sensors, 23(23), 9317.
11. Obuseh, E., Eyenubo, J., Alele, J., Okpare, A., & Oghogho, I. (2025). A systematic review of barriers

to renewable energy integration and adoption. Journal of Asian Energy Studies, 9, 26-45.

12. Oghenegare, A. J., Nkemdilim, E. J., Ewere, O. E., Donald, I., & Ekene, M. C. (2024). Renewable Energy in Nigeria: A comprehensive examination of the viability of solar energy in Nigeria. International Journal of Innovative Research in Technology, 11(5), 2438-2433.
13. Otuagoma, S., Obuseh, E., Akpovi, O., Okpare, A., Eyenubo, J., & Roland, T. (2025). Assessment of Conveyor Telemetry System in a Manufacturing Firm: A Case Study of a Brewery in Eastern Nigeria. NIPES-Journal of Science and Technology Research, 7(2), 44-58.
14. Wang, R., Huang, Z., Yang, Y., Wen, Y., & Sun, X. (2025). A review on robust predictive control of permanent magnet synchronous motor drives: Strategies and future trends. AIP Advances, 15(11).
15. Yi, P., Zheng, W., & Li, X. (2024). Overview of torque ripple minimization methods for permanent magnet synchronous motors based on harmonic injection. Chinese Journal of Electrical Engineering, 10(2), 16-29.